

RESEARCH ARTICLE OPEN ACCESS

Tuning Nanoparticle Microstructure through Nanodroplet-Mediated Electrodeposition: Applications to PtCu Alloy Nanoparticle Synthesis and Electrocatalysis

Saptarshi Paul¹ | John F. Koons¹ | Michael L. Harrigan¹ | Kingshuk Roy^{2,3} | Jeffrey E. Dick^{1,4} 

¹Department of Chemistry, Purdue University, West Lafayette, Indiana, USA | ²Research Institute for Sustainable Energy, TCG Centres for Research and Education in Science and Technology, Salt Lake, India | ³Academy of Scientific and Innovative Research (AcSIR), Ghaziabad, India | ⁴Elmore Family School of Electrical and Computer Engineering, Purdue University, West Lafayette, Indiana, USA

Correspondence: Jeffrey E. Dick (jdick@purdue.edu)

Received: 21 February 2025 | **Revised:** 21 February 2025 | **Accepted:** 5 March 2025

Funding: National Science Foundation CAREER, Grant/Award Number: CHE-2045672

ABSTRACT

Nanoparticles are an indispensable part of our lives. From electronic devices to drug delivery to catalysis and energy storage, nanoparticles have found various important applications. Out of the many synthetic strategies to generate nanoparticles, electrodeposition has stood out due to its cost effectiveness, low time consumption and simplicity. However, traditional electrodeposition techniques have suffered from controlling the size, shape, morphology and microstructure of nanoparticles. Here, we use a technique called nanodroplet-mediated electrodeposition, where nanodroplets carrying the metal salt precursor collide with a negatively-biased electrode. In this work, we use this nanodroplet-mediated electrodeposition technique along with transmission electron microscopy, selected-area electron diffraction and high-angle-annular dark-field scanning transmission electron microscopy to show control over the microstructure of single nanoparticles. Along with that, we use X-ray photoelectron spectroscopy to get mechanistic insights behind the alteration of microstructure observed. Having achieved a control over the microstructure, we show the application by synthesising polycrystalline alloys at room temperature and evaluating the electrocatalytic behavior of the different microstructures towards the hydrogen evolution reaction. This fundamental work of controlling microstructures of single nanoparticles and its applications in alloy synthesis and electrocatalysis opens a new avenue of tuning nanoparticles for various applications.

1 | Introduction

Nanoparticles possess unique properties that are quite different from bulk materials. They can exhibit high surface area-to-volume ratio, enhanced optical properties and quantum effects at the nanoscale [1, 2]. For example, the colour of gold nanoparticles depends on their shape and size. Smaller Au nanoparticles (10 nm–20 nm in size) appear red while larger particles shift towards a violet color [3, 4]. Thus, no two nanoparticles are the same. Therefore, studying fundamental properties of single nanoparticles is vital to realize the potential of nanoparticles

in catalysis and sensing applications [5–12]. On the same note, understanding the microstructure of single nanoparticles is important [9, 13–15]. Having an in-depth knowledge of the microstructure and how it is influenced by different parameters can guide us in utilizing these nanoparticles in a much more efficient way in the fields of catalysis [16, 17], energy storage devices [18] and biomedical applications [19].

Many synthetic pathways exist for nanomaterials of various shapes and sizes [20–22]. Electrodeposition is a very simple, less time-consuming and cost-effective way to produce single

This is an open access article under the terms of the [Creative Commons Attribution](https://creativecommons.org/licenses/by/4.0/) License, which permits use, distribution and reproduction in any medium, provided the original work is properly cited.

© 2025 The Author(s). *Electroanalysis* published by Wiley-VCH GmbH.

nanoparticles. However, due to diffusion layer overlap where the growing nucleus competes with neighbouring nuclei for metal salt precursor, it often leads to the formation of aggregate particles and thus lacks control over the microstructure of nanoparticles [23]. Nanodroplet-mediated electrodeposition has been on the rise due to its ability to overcome this issue and easily form single nanoparticles [24–26].

In nanodroplet-mediated electrodeposition, metal precursor salts are confined in a water droplet, which is suspended in an organic phase. As the droplets collide on the electrode surface, which is biased sufficiently negative to drive an electrochemical process, nanoparticles are formed. The contents of these droplets are electrolysed in milliseconds, and due to the fast mass transfer of this process, single-nucleation sites generally yield single particles. Previously, nanodroplet-mediated electrodeposition has been used to generate metal nanoparticles [24] and study their growth [25], morphology [24], porosity [24, 26] and other fundamental properties [26–30]. Glasscott et al. reported the formation of high-entropy alloys, which are amorphous in nature and obtained at high potentials (−1.5 V) [31]. Ahn's group has also reported the formation of metal oxides and hydroxides via aqueous nanodroplets at higher potentials due to interference with water reduction [32]. This blurs the line between electrodeposition and electroprecipitation, the process where an oxyhydroxide will precipitate because of a pH gradient. Thus, the question arises of whether we can tune the microstructure and composition of nanoparticles and their alloys based on the applied potential, and how would that tunability go on to affect the application of these nanoparticles in various domains. This knowledge gap is the focus of our work here.

In this work, we electrodeposit single-Pt nanoparticles using aqueous nanodroplets and demonstrate microstructure tunability by tuning the electrodeposition potential. We use high-angle-annular dark-field scanning transmission electron microscopy (HAADF-STEM), selected-area electron diffraction (SAED) and X-ray photoelectron spectroscopy (XPS) to analyze the microstructure of single nanoparticles at different applied potentials. This work gains a mechanistic insight via XPS into the change in microstructure observed as a function of potential,

and sheds light on the differentiation between electrodeposition and electroprecipitation.

We specifically probe the microstructure of the singular nanoparticles at different potentials to investigate the effect of side reactions (specifically water reduction in our case) on the electrodeposited nanoparticles. With the understanding gained, we show its application in the synthesis of polycrystalline alloys at room temperature and demonstrate the different electrocatalytic properties observed with the alteration of microstructure. Thus, we start from a fundamental viewpoint of tuning and understanding the alteration of microstructures in a single nanoparticle and go on to apply our understanding in different domains.

2 | Results and Discussion

Our primary objective was to elucidate the intricacies of nanoparticle microstructure and its modulation in response to varying electrochemical potentials. The electrode material used here is a glassy carbon electrode and was polished mechanically by alumina beads (of sizes typically varying from 5 to 0.05 μm) suspended in water (termed alumina slurry) to have a clean and smooth surface. We have used 0.1 M tetrabutylammonium perchlorate (TBAP) in dichloroethane (DCE) as our organic phase. Generally, we use a higher amount of electrolyte concentration compared to the analyte under study to reduce solution resistance and maintain electroneutrality via ion transfer, which can likely affect the deposition process. Our group has previously shown how different electrolytes like LiClO_4 can result in more spherical nanoparticle-like morphology [23].

Figure 1 illustrates our methodology, wherein we employed aqueous nanodroplets to deposit the nanoparticles. Specifically, we introduced 25 μL of the aqueous phase, containing the Pt precursor salt (H_2PtCl_6), into 5 mL of the organic phase, which was subsequently sonicated to yield aqueous nanodroplets. These nanodroplets, upon collision with the electrode, were subjected to different potentials to facilitate Pt nanoparticle deposition and microstructural examination.

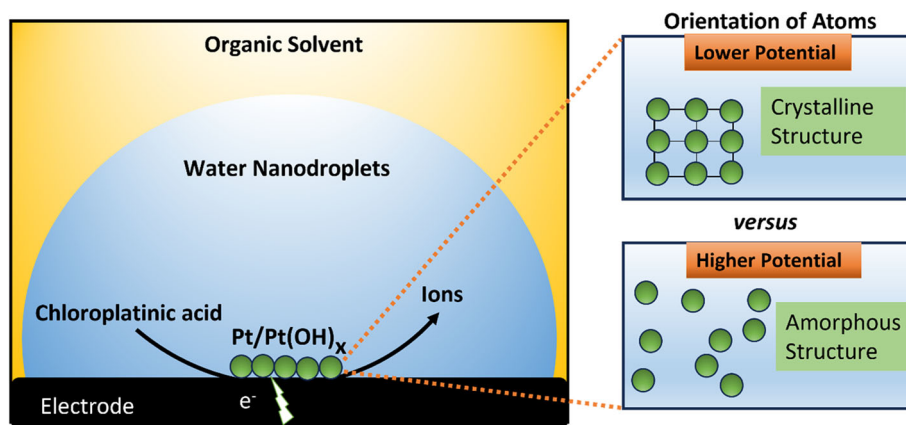


FIGURE 1 | Schematic representing the system of nanodroplet-mediated electrodeposition to form single nanoparticles, illustrating the microstructural variation of these nanoparticles with applied potential.

Guided by the linear sweep voltammetry (LSV) profile of Pt (Figure S1), we opted to apply a potential of -0.5 V, a choice substantiated by the LSV analysis to ensure adequate Pt deposition. Additionally, we explored Pt microstructures at -1.2 V, a potential where Pt deposition may interact with water reduction, potentially influencing microstructural attributes. The deposition process was conducted via amperometry for a duration of 240 s (Figure S2).

To scrutinize the microstructural variations at distinct potentials, we conducted TEM–SAED analyses. Figure 2a portrays a TEM image of a singular-Pt nanoparticle fabricated at -0.5 V, with Figure 2b showcasing its corresponding SAED pattern. The SAED pattern exhibits distinct rings with conspicuous bright spots, indicative of the material's polycrystalline nature. Conversely, Figure 2c displays a TEM image of a Pt nanoparticle synthesized at -1.2 V, accompanied by its SAED pattern in Figure 2d. Notably, the SAED pattern reveals a solitary ring devoid of any bright spots, signalling the amorphous character of these particles. Thus, discernible disparities in microstructure attributable to applied potential are evident. Multiple TEM–SAED results were considered (Figure S5) to come to this conclusion. In the upcoming discussion, we will also see how our TEM–SAED results match with our STEM–HAADF data.

Further investigations utilising HAADF–STEM were conducted to scrutinize the microstructure of Pt nanoparticles under varying potentials. In Figure 2e, we look at the nanoparticles at -0.5 V. Atomic lattices spanning the nanoparticle are discernible (highlighted by red lines), indicative of lattice ordering and thereby implying crystallinity. Conversely, at -1.2 V (Figure S4), the absence of discernible crystal lattices was seen—underscoring the amorphous nature of these nanoparticles. It is also important to note that the Miller indices extracted from the polycrystalline SAED pattern exhibit strong correlation with the d-spacing achieved from the HAADF image. The d-spacing achieved for the 101 planes in Figure 2d were 0.275 nm, which is close to the d-spacing of 0.265 nm achieved from HAADF. The calculations of these planes and d-spacing are given in Table S1. The findings from both TEM–SAED and HAADF–STEM analyses complement each other, collectively illustrating the observations of

microstructural alterations observed by inducing the applied potential. At -0.5 V, a more crystalline microstructure is observed, contrasting with the amorphous microstructure evident at -1.2 V. Furthermore, energy-dispersive X-ray (EDX) analyses (Figure S3) revealed a notable increase in oxygen content at -1.2 V compared to -0.5 V, indicative of Pt oxide or hydroxide species formation potentially stemming from electroprecipitation. In that respect, to deepen our understanding of these systems, we employed XPS for further investigation and analysis.

We performed XPS of the nanoparticles deposited at the two different potentials to get mechanistic insights for the results obtained. Figure 3a,b shows the fitted XPS peaks for Pt nanoparticles deposited at -0.5 and -1.2 V, respectively [33–35]. The peaks are assigned based on standard values (see Materials and Methods). In Figure 3a, we observe a higher amount of Pt (0) compared to Figure 3b. On the other hand, in Figure 3b, we observe a higher amount of Pt (II) than in Figure 3a. As the experiment is carried out in ambient conditions (presence of oxygen) and also due to the possibility of oxygen reduction reaction around -0.5 V, we do observe an appreciable amount of Pt (II) even at -0.5 V [36–38]. Nevertheless, we see a greater generation of Pt metal nanoparticles (Pt (0)) at -0.5 V and a higher amount of Pt oxyhydroxide species (Pt (II)) at -1.2 V which can be ascribed to the electroprecipitation of metal hydroxide species at higher potentials due to interference with water reduction [23, 31, 32]. Thus, the XPS data gives us a mechanistic insight in understanding the change in microstructure (amorphous to polycrystalline as shown before) observed at different potentials. This work sheds more light onto previous works done by Jeun [32], and Glasscott [31], by trying to separate electrodeposition from electroprecipitation at higher potentials. We have recently demonstrated that concurrent oxygen reduction with metal reduction can affect the morphology and composition of the resulting nanoparticles. Moreover, current work is being done by our group to understand the effect of oxygen and oxygen reduction on the morphology, microstructure and composition during electrodeposition of different nanoparticles [29]. Using the knowledge obtained, we extend our system to alloys and evaluate the electrocatalytic behavior of our material.

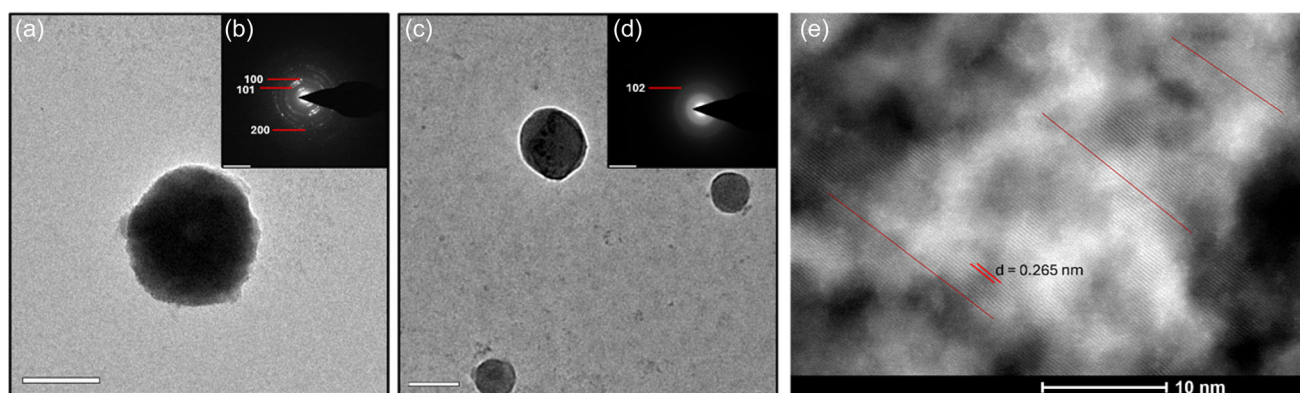


FIGURE 2 | (a,c) TEM image of a single nanoparticle electrodeposited at applied potentials of -0.5 V and -1.2 V versus Ag/AgCl, respectively. (b,d) Corresponding SAED pattern of a single nanoparticle depicted in (a,c), respectively. (e) HAADF–STEM image of nanoparticle electrodeposited at -0.5 V in (a) with 10 nm scale bar. (scale bar of TEM image: 100 nm (for both a and c); scale bar of SAED: 5 1/nm (for b); and 10 1/nm (for d) and 10 nm for (e)). SAED = selected-area electron diffraction; TEM = transmission electron microscopy; HAADF–STEM = high-angle-annular dark-field scanning transmission electron microscopy.

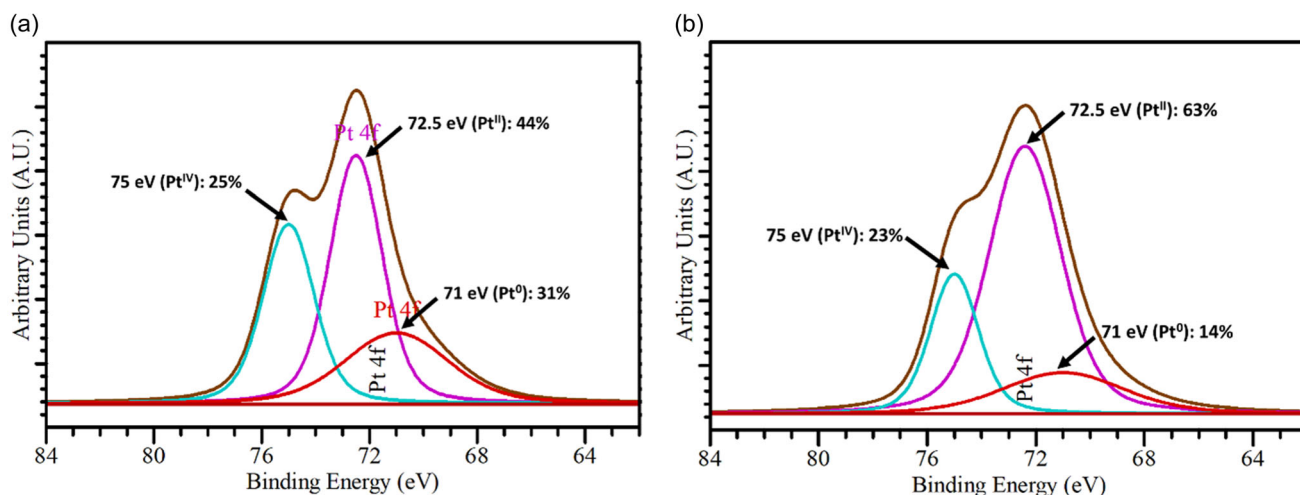


FIGURE 3 | (a,b) XPS data for Pt electrodeposited at -0.5 V and -1.2 V versus Ag/AgCl, respectively. XPS = X-ray photoelectron spectroscopy.

Having achieved an understanding of the alteration of the microstructures achieved at different potentials, we extended our system to alloys of Pt. Here, we considered CuPt alloys. We were able to achieve different microstructures of these alloys at different potentials. We used the same synthetic strategy of nanodroplet-mediated electrodeposition to synthesize alloys at -0.5 V and at -1.2 V.

Figure 4a (i) shows the HAADF-STEM image achieved at -0.5 V, (ii) shows its zoomed version and (iii) shows the SAED pattern of it. The HAADF-STEM image shows ordering of the crystals in different directions indicating polycrystallinity. The SAED pattern shows bright spots along with rings, which is also an indication of the polycrystalline nature of the alloy. Figure 4b

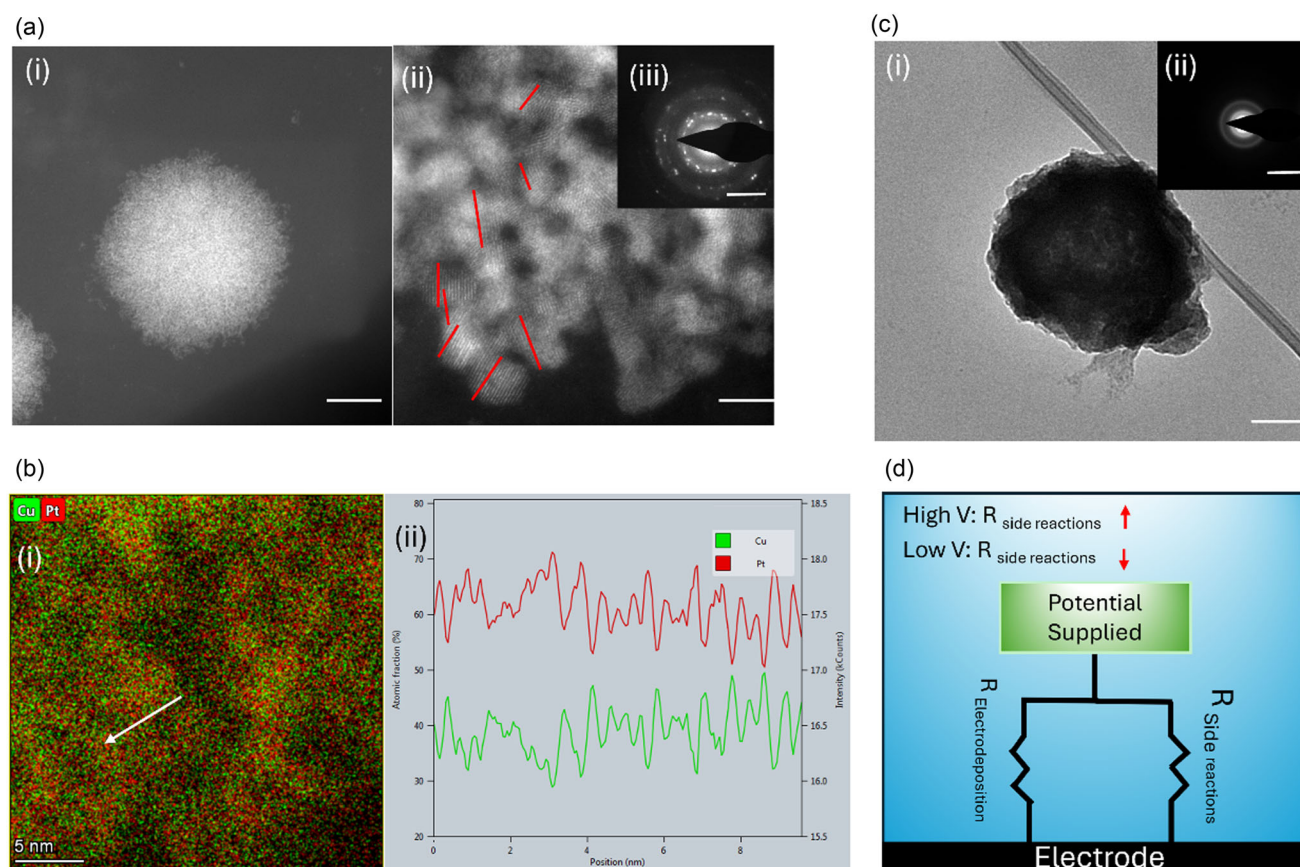


FIGURE 4 | (a) The electrodeposition of CuPt alloy at -0.5 V: (i) HAADF-STEM image, (ii) higher magnification HAADF-STEM image and (iii) corresponding SAED pattern; (b) (i) EDX mapping and (ii) EDX linescan of the CuPt alloy. (c) (i) TEM image of an amorphous alloy and (ii) the SAED pattern of it. (d) Circuit diagram differentiating deposition from side reactions. (scale bar: 50 nm for TEM image in a (i) and c (i); 5 nm in a (ii); SAED patterns for a (iii) and c (ii) are 5 1/nm; b (i) is 5 nm). EDX = energy-dispersive X-ray; HAADF = high-angle-annular dark field; STEM = scanning transmission electron microscopy; SAED = selected-area electron diffraction; TEM = transmission electron microscopy.

(i) shows the EDX mapping of the CuPt alloy and (ii) shows the linescan across the white arrow in the mapping image. The mapping depicts a very homogeneous distribution of the CuPt alloy and the linescan shows that almost every crest of Cu/Pt is met with a trough of Pt/Cu, indicating the homogeneous nature of the alloy. This indicates the formation of a solid solution alloy. The fast mass transfer of the nanodroplet-mediated electrodeposition process (electrolysis in milliseconds) and the similar electrodeposition onset potential for both Cu and Pt (Figure S8) help in achieving this solid solution-like structure. In Figure 4c (i), we see a TEM image at -1.2 V and its consequent SAED pattern in (ii). SAED pattern lacks the presence of any bright spots and only shows diffused rings, an indication of the amorphous nature of the alloys. TEM-SAED and HAADF-STEM of other nanoparticles at these potentials are provided in Figures S6 and S7.

Thus, we observe the separation of polycrystalline and amorphous alloys based on the potentials applied. It again hints at the interference of water reduction reaction at higher potentials which brings about this change in crystallinity. To explain this phenomenon, we drew a schematic in Figure 4d which shows the distribution of charge to different reactions based on the potential applied. At lower potentials, most of the charge is used for the electrodeposition process of the nanoparticles/alloys, but at higher potentials, a part of it may be used by other side reactions (in our case, water reduction reaction). This distribution of charge to different reactions and their consequent interference in the electrodeposition process seems to be the reason behind the difference in crystallinity that we are observing. It is also important to note here that by understanding this phenomenon, we are able to synthesize polycrystalline alloys at room temperature. Generally, polycrystalline alloys are synthesized at high temperatures via methods like chemical vapor deposition, physical vapor deposition, sol-gel or other thermal methods [39]. But here, taking advantage of the nanodroplet mediated electrodeposition method and being able to have control over the microstructure of the nanoparticles, we are able to synthesize polycrystalline alloys at room temperature. Not only that but these polycrystalline alloys also went on to show solid solution like features, as discussed before. After understanding the effect of side reactions and the distribution of potential in the alteration of the microstructure observed both for single nanoparticles and their alloys, we go on to probe how this affects their electrocatalytic behavior.

Investigations towards the hydrogen evolution reaction (HER) are in great demand as it is believed to be at the center of renewable energy. Pt is seen as the best catalyst for HER [40, 41]. Here, we depict the effect of the crystallinity of Pt as well as of its alloys on their electrocatalytic activity towards HER. To compare the electrocatalytic behavior, we set a baseline at 10 mA/cm^2 and see the corresponding overpotential observed. This method of comparing overpotential of different materials to see their electrocatalytic property has been benchmarked before [42]. From Figure 5 we observe that polycrystalline Pt nanoparticles (green) give an overpotential of -0.56 V compared to an overpotential of -0.63 V for amorphous Pt nanoparticles (blue). Similarly, we also observe that polycrystalline alloy nanoparticles of CuPt (black) performed slightly better with an overpotential of -0.76 V compared to that of amorphous CuPt alloy nanoparticles (red) which shows an overpotential of -0.78 V. The purple line denotes bare glassy carbon electrode without any deposition performed as a

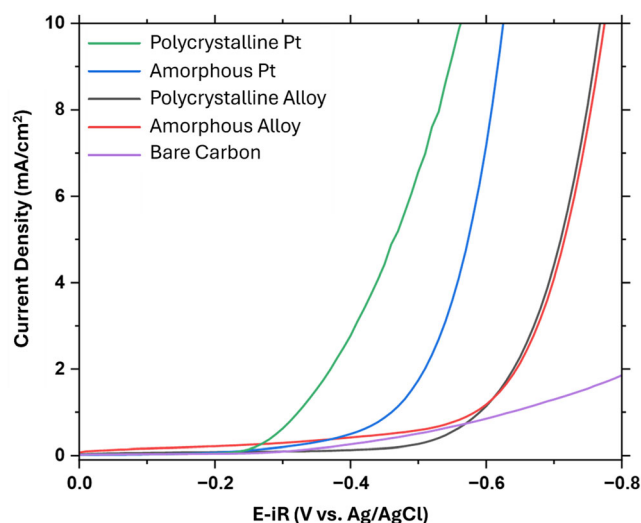


FIGURE 5 | The electrocatalytic behaviour towards the HER for polycrystalline and amorphous nanoparticles as well as polycrystalline and amorphous nanoparticle alloys against a reference of glassy carbon electrode. HER = hydrogen evolution reaction.

control. The performance of the alloy nanoparticles is worse than that of Pt nanoparticles. As Pt is the best-performing electrocatalytic material, any alloy is expected to be subpar with respect to pure Pt. The reason for the polycrystalline alloy nanoparticles performing better than amorphous alloy nanoparticles might be attributed to the higher generation of Pt oxide or hydroxide (Pt (II)) nanoparticles at elevated potentials than Pt metal (Pt (0)) nanoparticles as seen from the XPS data before. These oxide/hydroxide materials generated as a result of the water reduction reaction have a detrimental effect towards HER as compared to Pt metal nanoparticles [43]. Moreover, it has also been observed in literature that polycrystalline alloys have grain boundaries which help in promoting electrocatalytic behaviour [44–46]. This is an interesting electrocatalytic result we have observed as a function of crystallinity, which can be used later to tune nanoparticles to our needs. Leading from this, we find that one potentially exciting avenue of inquiry will be understanding how the multiphase microenvironment [47–49] influences metal electrodeposition [50–53].

3 | Conclusion

Nanodroplet-mediated electrodeposition has emerged as a promising technique for fabricating nanoparticles and probing their fundamental characteristics. In this study, we leveraged nanodroplet-mediated electrodeposition to investigate the evolution of microstructural properties in a singular nanoparticle under different applied potentials. Employing TEM-SAED and HAADF-STEM, we discerned a transition from a predominantly crystalline structure at lower potentials to a more amorphous configuration at higher potentials. Complementary insights into the underlying mechanisms were gleaned through XPS, elucidating the formation of Pt oxide or hydroxide species reminiscent of electroprecipitation, induced by interference with water reduction at elevated potentials. Having gained an understanding of the crystallinity difference observed at different potentials, we

went on to synthesize polycrystalline and amorphous alloys at room temperature and observed that the crystalline nanoparticles performed better than their amorphous counterparts. These studies highlight the potential of using nanodroplet-mediated electrodeposition to fine tune nanoparticles and their alloys for various applications.

Author Contributions

S.P., J.F.K., K.R. and J.E.D. wrote the manuscript. The concept of the paper was conceived by S.P. and J.E.D. All the electrochemical experiments were done by S.P. and J.F.K. S.P. did the electronic microscopic characterisations. K.R. analyzed the X-ray photoelectron spectroscopy data. M.L.H. helped in synthesis and characterisation of alloys and studying their catalytic property. S.P., J.F.K., M.L.H., K.R. and J.E.D. helped in the interpretation of the data. J.E.D. supervised all aspects of the work. All authors have agreed to the final version of the manuscript.

Acknowledgements

The authors would like to acknowledge the use of facilities within the Purdue Electron Microscopy Center Facility RRID SCR_022687. X-ray photoelectron spectroscopy data were obtained at the Surface Analysis Facility of the Birck Nanotechnology Center at Purdue University. The authors would like to acknowledge Dr. Zhongxia Shang from the Purdue Electron Microscopy Center. The authors acknowledge the support by the National Science Foundation CAREER under grant no. CHE-2045672.

Conflicts of Interest

The authors declare no conflicts of interest.

Data Availability Statement

The data that support the findings of this study are available from the corresponding author upon reasonable request.

References

1. S. Khan and M. K. Hossain, "Classification and Properties of Nanoparticles," in *Nanoparticle-Based Polymer Composites* (Elsevier, 2022), 15–54.
2. A. B. Asha and R. Narain, "Nanomaterials Properties," in *Polymer Science and Nanotechnology* (Elsevier, 2020), 343–359.
3. T. Jennings and G. Strouse, "Past, Present, and Future of Gold Nanoparticles," *Bio-Applications of Nanoparticles* 620 (2007): 34–47.
4. R. Wilson, "The Use of Gold Nanoparticles in Diagnostics and Detection," *Chemical Society Reviews* 37, no. 9 (2008): 2028–2045.
5. W. Wang and N. Tao, "Detection, Counting, and Imaging of Single Nanoparticles," *Analytical Chemistry* 86, no. 1 (2014): 2–14, <https://doi.org/10.1021/ac403890n>.
6. Y. Song, Z. Zhang, H. E. Elsayed-Ali, et al., "Identification of Single Nanoparticles," *Nanoscale* 3, no. 1 (2011): 31–44.
7. Y. Wang, X. Shan, and N. Tao, "Emerging Tools for Studying Single Entity Electrochemistry," *Faraday Discussions* 193 (2016): 9–39.
8. O. J. Wahab, M. Kang, and P. R. Unwin, "Scanning Electrochemical Cell Microscopy: A Natural Technique for Single Entity Electrochemistry," *Current Opinion in Electrochemistry* 22 (2020): 120–128.
9. J. B. Sambur and P. Chen, "Approaches to Single-Nanoparticle Catalysis," *Annual Review of Physical Chemistry* 65 (2014): 395–422.
10. S. Nie and S. R. Emory, "Probing Single Molecules and Single Nanoparticles by Surface-Enhanced Raman Scattering," *Science* 275, no. 5303 (1997): 1102–1106.
11. A. J. Haes, D. A. Stuart, S. Nie, and R. P. Van Duyne, "Using Solution-Phase Nanoparticles, Surface-Confined Nanoparticle Arrays and Single Nanoparticles as Biological Sensing Platforms," *Journal of Fluorescence* 14 (2004): 355–367.
12. T. Huang and X.-H. N. Xu, "Synthesis and Characterization of Tunable Rainbow Colored Colloidal Silver Nanoparticles Using Single-Nanoparticle Plasmonic Microscopy and Spectroscopy," *Journal of Materials Chemistry* 20, no. 44 (2010): 9867–9876.
13. W. Hong and C. W. Li, "Microstructural Evolution of Au@ Pt Core-Shell Nanoparticles under Electrochemical Polarization," *ACS Applied Materials & Interfaces* 11, no. 34 (2019): 30977–30986.
14. C. Liu, J. Xu, C. Jiang, H. Gao, X. Ren, and L. Lu, "The Microstructure-Activity Relationship of Metal-Organic Framework-Based Electrocatalysts for the Oxygen Evolution Reaction at the Single-Particle Level," *ACS Materials Letters* 5 (2023): 1902–1910.
15. Z. Chen, Z. Jiao, D. Pan, et al., "Recent Advances in Manganese Oxide Nanocrystals: Fabrication, Characterization, and Microstructure," *Chemical Reviews* 112, no. 7 (2012): 3833–3855.
16. A. T. Vu and T. A. T. Pham, "Study on Method of Doping Au Nanoparticles on ZnO Stratified Microstructure to Enhance Photocatalytic Ability and Antibacterial Activity," *Bulletin of Chemical Reaction Engineering & Catalysis* 18, no. 1 (2023): 131–150.
17. S. Schauermaun, N. Nilius, S. Shaikhutdinov, and H.-J. Freund, "Nanoparticles for Heterogeneous Catalysis: New Mechanistic Insights," *Accounts of Chemical Research* 46, no. 8 (2013): 1673–1681.
18. L. Zhang, Y. Jing, P. Qu, W. Wang, X. Yao, and L. Tian, "Effect of Microstructure of Nanoparticles and Surrounding Alcohol Groups on Energy Transfer Efficiency," *Applied Thermal Engineering* 215 (2022): 119031.
19. D. Qiu, X. An, Z. Chen, and X. Ma, "Microstructure Study of Liposomes Decorated by Hydrophobic Magnetic Nanoparticles," *Chemistry and Physics of Lipids* 165, no. 5 (2012): 563–570.
20. A. Bapat, C. Anderson, C. R. Perrey, C. B. Carter, S. A. Campbell, and U. Kortshagen, "Plasma Synthesis of Single-Crystal Silicon Nanoparticles for Novel Electronic Device Applications," *Plasma Physics and Controlled Fusion* 46, no. B97 (2004): 12B.
21. S. Bhaviripudi, E. Mile, S. A. Steiner, et al., "CVD Synthesis of Single-Walled Carbon Nanotubes from Gold Nanoparticle Catalysts," *Journal of the American Chemical Society* 129, no. 6 (2007): 1516–1517.
22. S. Ji, Y. Chen, X. Wang, Z. Zhang, D. Wang, and Y. Li, "Chemical Synthesis of Single Atomic Site Catalysts," *Chemical Reviews* 120, no. 21 (2020): 11900–11955.
23. J. Reyes-Morales and J. E. Dick, "Electrochemical-Shock Synthesis of Nanoparticles from Sub-Femtoliter Nanodroplets," *Accounts of Chemical Research* 56, no. 10 (2023): 1178–1189, <https://doi.org/10.1021/acs.accounts.3c00050>.
24. M. W. Glasscott, A. D. Pendergast, and J. E. Dick, "A Universal Platform for the Electrodeposition of Ligand-Free Metal Nanoparticles from a Water-in-Oil Emulsion System," *ACS Applied Nano Materials* 1, no. 10 (2018): 5702–5711, <https://doi.org/10.1021/acsnano.8b01308>.
25. M. W. Glasscott, C. M. Hill, and J. E. Dick, "Quantifying Growth Kinetics of Single Nanoparticles in Sub-Femtoliter Reactors," *The Journal of Physical Chemistry C* 124, no. 26 (2020): 14380–14389, <https://doi.org/10.1021/acs.jpcc.0c03518>.
26. M. W. Glasscott and J. E. Dick, "Fine-Tuning Porosity and Time-Resolved Observation of the Nucleation and Growth of Single Platinum Nanoparticles," *ACS Nano* 13, no. 4 (2019): 4572–4581, <https://doi.org/10.1021/acsnano.9b00546>.

27. S. Paul, J. Reyes-Morales, K. Roy, and J. E. Dick, "Anodic Electrodeposition of IrOx Nanoparticles from Aqueous Nanodroplets," *ACS Nanoscience Au* 4, no. 3 (2024): 216–222, <https://doi.org/10.1021/acsnanoscienceau.3c00061>.
28. J. Reyes-Morales, S. Paul, M. Vullo, M. Q. Edwards, and J. E. Dick, "Room Temperature Electrochemical-Shock Synthesis of Solid-Solution Medium-Entropy Alloy Nanoparticles for Hydrogen Evolution," *Langmuir* 40, no. 46 (2024): 24272–24280.
29. J. F. Koons, S. Paul, and J. E. Dick, "Oxygen Reduction Allows Morphology-Tunable Copper Nanoparticle Electrodeposition from Aqueous Nanodroplets," *Langmuir* 41, (2025): 5524–5533.
30. J. Reyes-Morales, B. T. Vanderkwaak, and J. E. Dick, "Enabling Practical Nanoparticle Electrodeposition from Aqueous Nanodroplets," *Nanoscale* 14, no. 7 (2022): 2750–2757.
31. M. W. Glasscott, A. D. Pendergast, S. Goines, et al., "Electrosynthesis of High-Entropy Metallic Glass Nanoparticles for Designer, Multi-Functional Electrocatalysis," *Nature Communications* 10, no. 1 (2019): 2650, <https://doi.org/10.1038/s41467-019-10303-z>.
32. Y. E. Jeun, B. Baek, M. W. Lee, and H. S. Ahn, "Surfactant-Free Electrochemical Synthesis of Metallic Nanoparticles via Stochastic Collisions of Aqueous Nanodroplet Reactors," *Chemical Communications* 54, no. 72 (2018): 10052–10055, <https://doi.org/10.1039/C8CC05760E>.
33. A. S. Arico, A. K. Shukla, H. Kim, S. Park, M. Min, and V. Antonucci, "An XPS Study on Oxidation States of Pt and Its Alloys with Co and Cr and Its Relevance to Electroreduction of Oxygen," *Applied Surface Science* 172, no. 1–2 (2001): 33–40.
34. E. I. Vovk, A. V. Kalinkin, M. Y. Smirnov, I. O. Klembovskii, and V. I. Bukhtiyarov, "XPS Study of Stability and Reactivity of Oxidized Pt Nanoparticles Supported on TiO₂," *The Journal of Physical Chemistry C* 121, no. 32 (2017): 17297–17304.
35. Z. Paál and R. Schlögl, "XPS and UPS of Pt Catalysts of Different Preparation," *Surface and Interface Analysis* 19, no. 1–12 (1992): 524–528.
36. Y. Nie, L. Li, and Z. Wei, "Recent Advancements in Pt and Pt-Free Catalysts for Oxygen Reduction Reaction," *Chemical Society Reviews* 44, no. 8 (2015): 2168–2201.
37. N. M. Marković, T. J. Schmidt, V. Stamenković, and P. N. Ross, "Oxygen Reduction Reaction on Pt and Pt Bimetallic Surfaces: A Selective Review," *Fuel Cells* 1, no. 2 (2001): 105–116.
38. A. M. Gómez-Marín, R. Rizo, and J. M. Feliu, "Oxygen Reduction Reaction at Pt Single Crystals: A Critical Overview," *Catalysis Science & Technology* 4, no. 6 (2014): 1685–1698.
39. D. W. Ma and C. Cheng, "Preparations and Characterizations of Polycrystalline PbSe Thin Films by a Thermal Reduction Method," *Journal of Alloys and Compounds* 509, no. 23 (2011): 6595–6598.
40. Z. Li, J.-Y. Fu, Y. Feng, C.-K. Dong, H. Liu, and X.-W. Du, "A Silver Catalyst Activated by Stacking Faults for the Hydrogen Evolution Reaction," *Nature Catalysis* 2, no. 12 (2019): 1107–1114.
41. A. Eftekhari, "Electrocatalysts for Hydrogen Evolution Reaction," *International Journal of Hydrogen Energy* 42, no. 16 (2017): 11053–11077.
42. C. C. L. McCrory, S. Jung, I. M. Ferrer, S. M. Chatman, J. C. Peters, and T. F. Jaramillo, "Benchmarking Hydrogen Evolving Reaction and Oxygen Evolving Reaction Electrocatalysts for Solar Water Splitting Devices," *Journal of the American Chemical Society* 137, no. 13 (2015): 4347–4357, <https://doi.org/10.1021/ja510442p>.
43. J. N. Hansen, H. Prats, K. K. Toudahl, et al., "Is There Anything Better than Pt for HER?," *ACS Energy Letters* 6, no. 4 (2021): 1175–1180.
44. X. Xu, Y. Zhong, M. Wajrak, T. Bhatelia, S. P. Jiang, and Z. Shao, "Grain Boundary Engineering: An Emerging Pathway toward Efficient Electrocatalysis," *InfoMat* 6, no. 8 (2024): e12608.
45. S. Zhang, B. Gao, S. Sun, et al., "The Study of the Effects of Grain Size, Orientation and Dislocation Density on the HER Performance of Copper Catalysts," *Journal of Alloys and Compounds* 1002 (2024): 175255.
46. S. Mondal, S. K. De, R. Jana, et al., "Unveiling the Excellent Electrocatalytic Activity of Grain-Boundary Enriched Anisotropic Pure Gold Nanostructures toward Hydrogen Evolution Reaction: A Combined Approach of Experiment and Theory," *ACS Applied Energy Materials* 4, no. 4 (2021): 3017–3032.
47. L. E. Krushinski and J. E. Dick, "Direct Electrochemical Evidence Suggests that Aqueous Microdroplets Spontaneously Produce Hydrogen Peroxide," *Proceedings of the National Academy of Sciences of the United States of America* 121, no. 12 (2024): e2321064121.
48. L. E. Krushinski, P. J. Herchenbach, and J. E. Dick, "The Gas| Liquid Interface Eclipses the Liquid| Liquid Interface for Glucose Oxidase Rate Acceleration in Microdroplets," *Proceedings of the National Academy of Sciences of the United States of America* 121, no. 51 (2024): e2416353121.
49. L. E. Krushinski, K. J. Vannoy, and J. E. Dick, "Single Liquid Aerosol Microparticle Electrochemistry on a Suspended Ionic Liquid Film," *Small* 20, no. 28 (2024): 2308637.
50. G. S. Colón-Quintana, T. B. Clarke, and J. E. Dick, "Interfacial Solute Flux Promotes Emulsification at the Water| Oil Interface," *Nature Communications* 14, no. 1 (2023): 705.
51. G. Colón-Quintana, T. B. Clarke, S. A. Ailawar, and J. E. Dick, "Single Gold Nanowires with Ultrahigh (>10⁴) Aspect Ratios by Triphasic Electrodeposition," *Nanoscale* 16, no. 43 (2024): 20073–20081.
52. G. Colón-Quintana and J. E. Dick, "Voltage-Driven Ion Flux Promotes Emulsification at the Water| Oil Interface," *Materials Horizons* 10, no. 11 (2023): 4986–4991.
53. T. B. Clarke, L. E. Krushinski, K. J. Vannoy, et al., "Single Entity Electrocatalysis," *Chemical Reviews* 124, no. 15 (2024): 9015–9080.

Supporting Information

Additional supporting information can be found online in the Supporting Information section.